ARTICLE

OPEN

Check for updates

Global mining footprint mapped from high-resolution satellite imagery

Liang Tang [1] & Tim T. Werner [2]✉

Mining is of major economic, environmental and societal consequence, yet knowledge and understanding of its global footprint is still limited. Here, we produce a global mining land use dataset via remote sensing analysis of high-resolution, publicly available satellite imagery. The dataset comprises 74,548 polygons, covering ~66,000 km^2 of features like waste rock dumps, pits, water ponds, tailings dams, heap leach pads and processing/milling infrastructure. Our polygons finely contour the edges of mine features and do not include the space between them. This distinguishes our dataset from others that employ broader definitions of mining lands. Hence, despite our database being the largest to date by number of polygons, comparisons show relatively lower global land use. Our database is made freely available to support future studies of global mining impacts. A series of spatial analyses are also presented that highlight global mine distribution patterns and broader environmental risks.

[1] College of Earth Sciences, Chengdu University of Technology, 610059 Chengdu, China. [2] School of Geography, Earth and Atmospheric Sciences, Faculty of Science, The University of Melbourne, Carlton, VIC, Australia. ✉email: tim.werner@unimelb.edu.au

Extractive industries can dramatically alter landscapes and cause irreversible damage to surrounding environments and communities. They simultaneously promise economic and social development and are essential to many key supply chains[1,2]. As mine areas continue their expansion across the globe, there is an increasing need for research that identifies impacts on surrounding landscapes. A subset of this research uses GIS and remote sensing methods to map the extent of land transformation due to mining activity[3–9]. These mapping exercises foster a more sophisticated understanding of the scale and location of risks posed by mining activity from local to global scales. They can also permit more nuanced planning of future developments in mining regions, for example, by informing the likely scale of future mine developments when mineral discoveries are made.

Research on the spatial patterns of mining can be mine- or region-specific[6,10], or may examine mining as a global geographic phenomenon[11,12]. Global-scale studies have often relied on global corporate mining databases such as the Standard & Poor's SNL metals and mining database[13] and review studies in economic geology (e.g.,[14,15]) that provide data on the coordinates of larger-scale mines. However, delineating the complete area occupied by mines at each coordinate is a comparatively more complex endeavor. Typically, it requires visual inspection or machine learning analysis of satellite imagery, followed by validation of mapped areas using alternative satellite imagery, corporate data, and/or field investigations. Studies like Yang et al.[16] and Yu et al.[17] have sought to use image processing algorithms to automatically identify and delineate mine areas, typically based on an already known dataset of mine areas. However, such studies typically focus on single regions, as the environments in which mines operate can be so variable that applying a singular visual approach or training dataset entails considerable uncertainty between different mining regions. On a global scale, studies like Tang et al.[8], Werner et al.[3], and Maus et al.[7] have recently employed manual visual inspection methods to delineate mines as polygons. These studies have employed slightly different approaches to classifying mine areas, yet collectively have improved the global coverage of sites mapped and sought to increase the precision of estimates for already mapped areas. The most recent of these efforts by Maus et al.[18] contributed around 44,929 polygons of global mining areas. Below, we outline an update that builds on these efforts to provide a mine area polygon dataset significantly larger (by the number of polygons) than any previous study. It therefore offers an advanced spatial dataset that progresses toward comprehensive and refined mapping of global mining land use. In the following sections, we explain our approach to updating global mine area data and provide a series of spatial analyses. We also compare to other global mining land use studies to illustrate differences in methodology and understandings of what comprises the global mining footprint. These comparisons allow for methodological refinement and replicability in future mapping endeavors. Our analyses indicate hot- and cold-spots of global mining activity, explain patterns occurring at large- and small-scales of mining, and show the enormous potential differences between areas occupied by mining itself, versus the broader areas impacted by mining. The complete polygon dataset is available for download via Zenodo, at https://doi.org/10.5281/zenodo.6806817.

Results and discussion

Global mine areas and mine sites. 74,548 mine area polygons are reported in the present study, with global coverage and example delineated areas illustrated in Fig. 1. A total estimated mine area of 65,585.4 km^2 is mapped, with an arithmetic mean of 0.88 km^2

(258,493.0 km total perimeter, 3.5 km/polygon). Figure 1 shows that while mines are composed of common features including (but not limited to) pits, waste rock dumps, water ponds, ore stockpiles, processing infrastructure and tailings dams, they show considerable variability in their spatial forms and scales. Table 1 summarizes areas from the most prominent mining nations. Our dataset comprises mine area polygons from 135 countries and regions, though these areas are highly clustered. Approx. 79% of the polygons are situated within 13 countries: China, USA, Russia, Australia, Indonesia, South Africa, Ukraine, Ghana, Canada, India, Brazil, Kazakhstan, and Chile. Correspondingly, 122 countries and regions have ~21% of the total mine area polygons, with fewer than 625 polygons each (<1%). Major mining nations can broadly be divided into high mineral demand countries (e.g., China, India, and USA) and high mineral export countries (e.g., Australia, Canada, South Africa, and Russia). Naturally, mine areas are situated in highly diverse geological, socio-political and environmental contexts. For example, mine areas in Ukraine arise from intensive coal exploration in the Soviet period[7], and Ghana's mine areas largely arise from placer gold resources in local riverine environments[19].

An overlay analysis of mine polygons versus SNL database coordinates showed that 58% of our polygons intersected with the 10 km buffers of 12,179 known mine operations. Of these, 9023 are "Active", 1802 "Inactive", and the remainder classified as "Care and Maintenance", "Rehabilitation", "Under Litigation" or "On Hold". This compares to 6201 "Active" sites covered in Maus et al.[7], which was subsequently updated with approx. double the count of polygons in Maus et al.[18], but without updating the specific number of sites represented. The extent of overlap with SNL data on a per-commodity basis is presented in supplementary Table S1.

Spatial distribution characteristics. To further explore global distribution patterns, we equally subdivided global land areas into 8,653 equal rectangular cells (fishnets[20]), with an average area of 15,400 km^2 per cell. Mine area polygons were mapped to 2021 of these fishnets, revealing that mine area densities range from 0 to 16.1% per fishnet, at an average of 0.028%. Colder regions (e.g., northern Canada, Russia, and Greenland), high altitude areas (e.g., Qinghai-Tibet Plateau, China), and arid regions with limited resource demands (e.g., Afghanistan, Arabian Peninsula, Sahara Desert) exhibited lower mine area density. The former is potentially explained by hazardous climatic conditions that inhibit large-scale mining and exploration, and the latter is correlated with limited population. Reduced mine density in inland Africa is potentially an artefact of limited public reporting that inhibits the identification of small-scale mining. With rare exceptions, intensive mining is conducted ~4000 m above the sea level in Andes Belt, South America, which features a barbell vertical distribution[8]. By contrast, more mine areas are situated in mid-latitude regions, which corroborates increasing concerns linking mining to deforestation and environmental degradation[5,21,22]. Ultimately, the global distribution of mines is bound by the distribution of geological phenomena that concentrate minerals (e.g., geological fault zones, orogenic belts, great igneous provinces, and stable sedimentary basins) and the varying capacity for localities and companies to economically develop such sites, which is in turn influenced by a number of factors, including the depth of mineralization, and proximity to populations, roads and rail links[23].

In statistical terms, the Moran's I analysis of clustering behavior shows high index values both in global and local terms, indicating strong spatial autocorrelation behavior[24]. The Global Moran's I index of 0.115 is notably higher than Tang et al.[8]
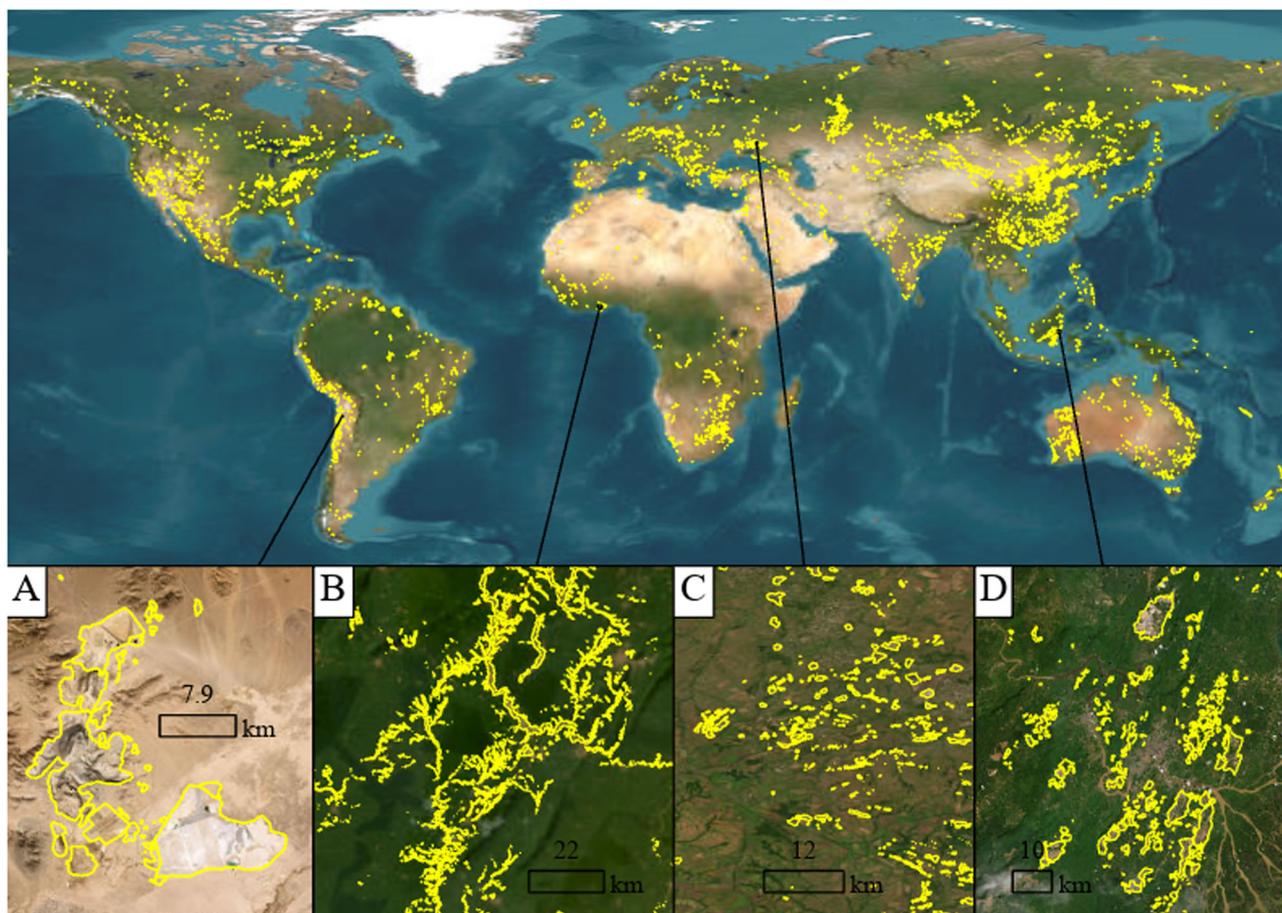
Fig. 1 Global mine area coverage, with cases of delineation of representative mine sites shown. A Larger open pit operations (Escondida mine, copper porphyry deposit, Chile, 24°16′15 S, 69°4′14 W); **B** Formal/artisanal placer gold mining, Ankobra River, Ghana, where all mining sites are along the riversides or in the riverbed, forming a dendritic configuration (5°43′ N, 2°6′ W). **C** Coal mine sites and gangue heaps in Donetsk, Ukraine (48°12′ N, 38°39′ E); **D** Coal mine areas surrounding Samarinda in East Kalimantan, Indonesia (0°29′48 S 117°08′10 E). Imagery credit: Esri, Maxar, and Earthstar Geographics.

Table 1 Summary of per-country mine areas mapped in this study.				
Countries	**Polygons**	**Occupied land (km^2)**	**Average (km^2/ polygon)**	**Standard deviation (km^2/ polygon)**
China	29348	7887.85	0.27	1.59
USA	6053	8499.04	1.4	5.45
Russia	4659	8675.45	1.86	5.72
Australia	4046	5319.70	1.31	4.74
Indonesia	2117	3689.83	1.74	10.22
South Africa	1984	3021.75	1.52	4.45
Ukraine	1931	1348.92	0.7	7.56
Ghana	1894	998.01	0.53	2.46
Canada	1890	3318.95	1.76	8.09
India	1795	2067.70	1.15	4.78
Brazil	1303	1395.33	1.07	3.08
Kazakhstan	1089	1722.26	1.58	3.53
Chile	839	2842.49	3.39	47.1
Other countries ($N = 122$)	15600	14798.10	0.99	4.65

(Global Moran's I index = 0.081). This is expected, as our study has increased global coverage and our method involved identification of additional mine areas adjacent to previously known features.

A map of local spatial autocorrelation patterns (Fig. 2) shows that NS clustering behavior was observed for 67.8% of land areas. LL clusters occupied 23.8% of the global land surface, followed by LH outliers (6.1%), HH clusters (1.2%), and HL outlier areas (1.1%, Fig. 2, see methodological descriptions for these cluster types below).

Assessing scales of mining activity. There is high variability in mine area scales, with a global standard deviation of 7.64 km^2. The sum of polygons presents a lognormal probability graph distribution and approximately straight lines[25]. This demonstrates that the data frequency distribution conforms to the lognormal distribution. The geometric mean (~0.123 km^2) may therefore best represent the average land occupied per mining feature (polygon).

Collectively, the quantity of mine sites varies substantially across scales (Fig. 3). An exponential decline is evident up to ~0.15 km^2, such that areas <0.15 km^2 account for 54.6% of all polygons. Mine areas from 1350 m^2 to 7200 m^2 are the most frequent, and the mode mine polygon size of 1800 m^2 accounts for ~0.54% of all mapped mine areas. Beyond 0.15 km^2, Fig. 3 shows a slight linear decrease. Mine areas also feature an S-curve accumulative tendency (logarithmic scale for the abscissa). The $\frac{K}{2}$
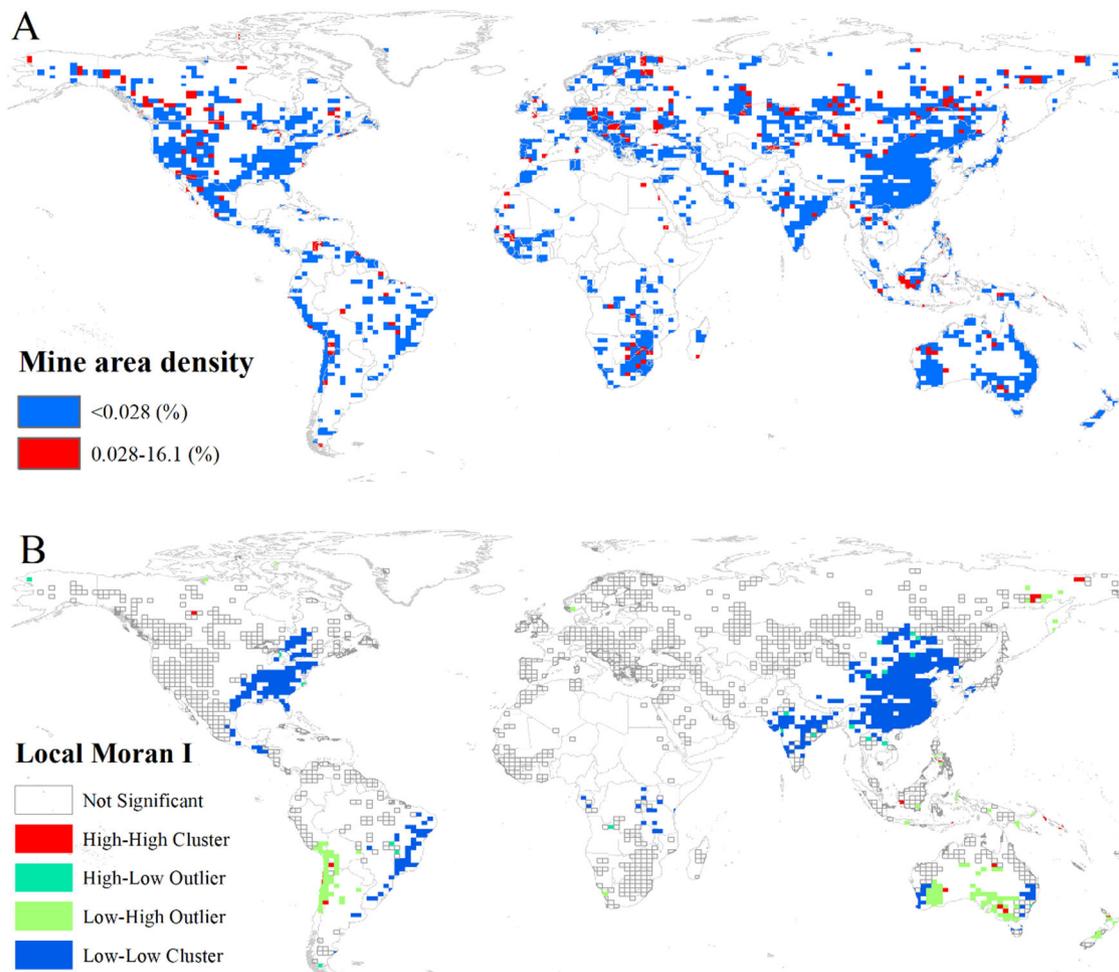
Fig. 2 Spatial heterogeneity of global mine areas. Global Moran's I index $= 0.115$, z-score $= 240$, p value < 0.001. Mine areas are aggregated to 8653 fishnet cells (15,400 km^2 per cell, with some cells bisected due to irregular coastal borders) projected to Interrupted Goode Homolosine. **A** The global distribution density of mapped mining areas; **B** Anselin Local Moran's I[55].

index of abscissa is equal to ~6.35 km^2, revealing those areas of around 6.35 km^2 account for the majority of total mine land use. Despite larger-scale mine sites remaining notably fewer in number, the scale of such mines still strongly influences total land occupation among the 74,548 mine polygons. By comparing with a smooth increasing curve in small-scale mine areas (e.g., <6.35 km^2 per mine site), the largest mine areas (>40 km^2 per mine site) show relatively jagged growth. In summary, while global mineral supply chains are dominated by the largest mines[3], minor-scale mining still contributes comparable areas to global mine land use.

Larger-scale mine areas may be characterized as including more than ~12.3 km^2 per polygon (per Fig. 3), and such sites represent the dominant share of global metals production[3]. On this basis, ~761 of the mine polygons mapped may be considered larger scale, corresponding to a total land use of 23,334.3 km^2 (35.6% of the total database area, averaging ~30.7 km^2 per polygon). These larger-scale mine areas are situated in 61 of the 135 countries mapped. By number of large-scale mine polygons, the national-level sequence is Russia ($n = 114$) > USA ($n = 97$) > Australia ($n = 67$) > China ($n = 58$) > Indonesia ($n = 51$) > Canada ($n = 50$) > Chile ($n = 35$) > South Africa ($n = 30$) > Colombia ($n = 22$) > Kazakhstan ($n = 22$) > Brazil ($n = 18$) > India (17) > other countries (180). Approx. 34 metals and nonmetals are produced from such sites (portions are poly-metallic deposits). The largest mine area is the Salar de Atacama

in Chile, as this site uniquely incorporates the broader salt flat from which lithium brines are pumped. In terms of the polygons by commodity, coal mining is the most prominent ($n = 304$, 7282.0 km^2), followed by gold ($n = 152$, 4623.1 km^2), copper ($n = 80$, 1722.6 km^2), iron ($n = 68$, 1339.0 km^2), phosphate ($n = 44$, 883.1 km^2), salt ($n = 21$, 2877.7 km^2), diamond ($n = 18$, 431.7 km^2), oil sands ($n = 16$, 738.1 km^2), bauxite ($n = 15$, 473.0 km^2), sand ($n = 11$, 249.6 km^2), uranium ($n = 7$, 123.3 km^2), and others ($n = 18$, 2591.1 km^2). As would be expected, the average polygon size (as opposed to total area) can also differ substantially between commodities. The largest mine type per polygon is a salt field (mean 137.03 km^2), which is typically situated in arid and inland regions. Other large types (on a per-polygon basis) include oil sands areas (46.13 km^2), which are mainly located in the Alberta province, Canada, and the large-scale bauxite mines (31.5 km^2), notably in northeast Australia, the Amazon Plain, and Kazakhstan.

ASM refers to mining by individuals, groups, families, or cooperatives, often in the market's informal (potentially illegal) sector[26]. While characteristically small on a per mine site or per polygon basis, the global ASM footprint is thought to be substantial. As such sites often do not comply with environmental regulations, the broader risks of these sites can be magnified[27]. ASM production has been estimated to account for 15–20% of the world's non-fuel minerals, 20% of gold, 40% of diamonds, and almost all colored gemstones[28,29]. However, the coverage of ASM
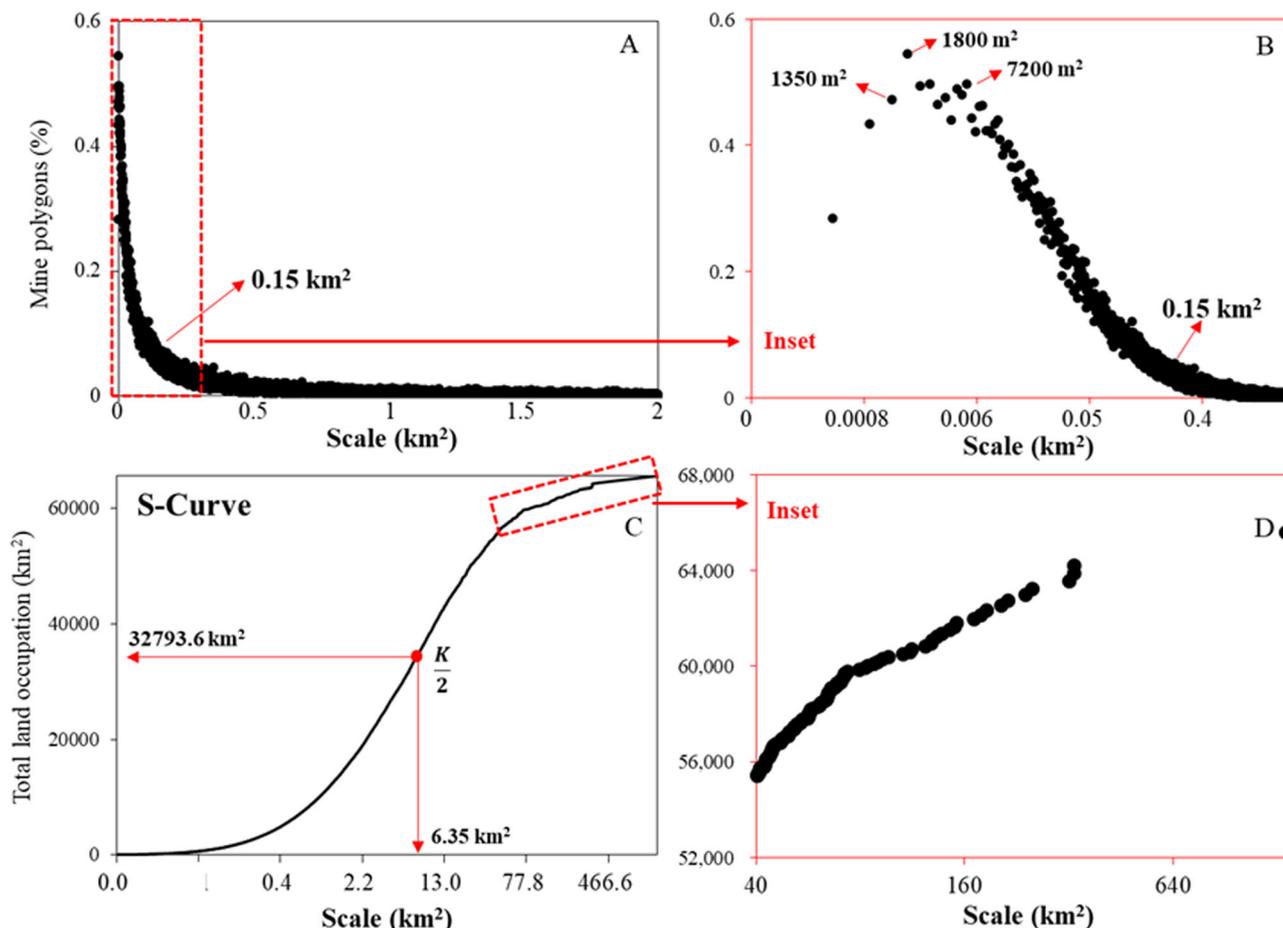
Fig. 3 Distribution of global mine area polygons by size. A Overall frequency distribution of mine area scales, noting that there may be under representation of polygons at the smallest scales due to limitations in ASM coverage; **B** Inset of small-scale mine areas; **C** S-curve of increasing total mine area versus the scale of mine polygons; **D** Inset of S-the curve of the largest-scale mine areas.

in past global mapping endeavors has been limited. It is therefore recognized that developing an understanding of the global ASM footprint is an important advancement. Table 2 presents the results of known ASM areas that were mapped in this study on a case study basis. We note that there is incomplete global coverage of ASM in our database. Some ASM areas require particularly high-resolution imagery and occasionally access to paid satellite services to appropriately analyze. Such sites can be difficult to include in a global-scale study due to their high dispersion. It is noted that national- and regional-scale studies have also mapped specific ASM areas, which we examine in the following section.

In this study, on a case study basis, we mapped 4058 polygons of ASM to examine the spatial characteristics of known small-scale, informal, and artisanal mining activity worldwide. These areas totaled 1071.2 km^2, constituting 1.63% of the total mine areas mapped (Table 3), yet are noted as representing only a portion of global ASM activity. For example, Asner et al.[10] estimate an additional 500 km^2 of small-scale gold mining in the Madre de Dios region of Peru alone.

ASM polygons in this study were highly variable in size, ranging from 0.0004 to 31.33 km^2, with arithmetic and geometric means of 0.264 km^2 and 0.062 km^2 per polygon respectively (Table 3). As the polygons fall approximately on a straight line in a lognormal probability graph, the geometric mean can represent the average scale of ASM[25]. ASM is ubiquitous in some of the developing countries assessed, including China, Ghana, Burkina Faso, Malawi, Mali, Mozambique, South Africa, Tanzania, Zambia, Zimbabwe, India, Indonesia, Papua New Guinea,

Philippines, Bolivia, Brazil, Ecuador, and Peru[26]. As large-scale mines are more likely to feature controlled mine waste site selection, comprehensive management, and post-mining rehabilitation works, elevated risks or environmental damage have emerged from ASM activities[30]. ASM areas are often associated with severe environmental, health, and safety risks[31–34], and the mapped land and riverbed areas subject to ASM did not exhibit apparent ecological protection measures. Thus, while the global large-scale metal mines covered substantially more land per polygon (≥12.3 km^2), the proportional impacts of ASM cannot be disregarded at any scale[3]. In some countries, ASM activity centers on the production of gold, bauxite, gemstones, iron ore, marble, and limestone[26], where related geological enrichment zones can lead to both formal and informal activity coexisting. Among the countries where ASM was prevalent, most activity was informal and considered illegal.

It should be noted, however, that it can be challenging to classify mine sites as ASM based on visual inspection alone, and indeed the proper definitions of such areas can also be unclear. As such, for the purposes of this study, we discuss areas based on a characteristic polygon size cutoff (~<0.062 km^2), visual appearance, and review of existing classifications of otherwise previously described ASM activity. Globally, a considerable portion of the formal mining areas appeared to host small-scale mining in surrounding areas. Yet some of these areas may incorporate the beginnings of new mineral excavation and construction of affiliated facilities. The land coverage of tailings ponds depends on the lifecycle of mining and may cover less land during early

Table 2 Extent of ASM regions mapped (km^2).

Study areas	Minerals	Polygons	Total area	Min	Max	Standard deviation	Median	Arithmetic mean	Geometric mean	External source (if relevant)
Manica, Mozambique	Gold	60	15.50	0.0045	2.58	0.408	0.114	0.258	0.100	31
Serra Pelada, Brazil	Gold	164	21.20	0.0025	1.46	0.177	0.073	0.129	0.069	
Jialingjiang basin, China	Pb-Zn, Cu	328	29.30	0.0004	1.99	0.198	0.029	0.089	0.030	58
Chengde, China	Iron	1719	240.49	0.0006	12.31	0.381	0.055	0.140	0.052	
Bonsa River, Ghana	Gold	1787	764.71	0.0008	31.33	1.638	0.072	0.428	0.082	
Summary of known ASM		4058	1071.2	0.0004	31.33	1.127	0.059	0.264	0.062	
Global small-scale mines[a]		27,410	665.3	0.0002	0.062	0.017	0.021	0.024	0.016	

[a]Based on mine polygons that are <0.062 km^2.
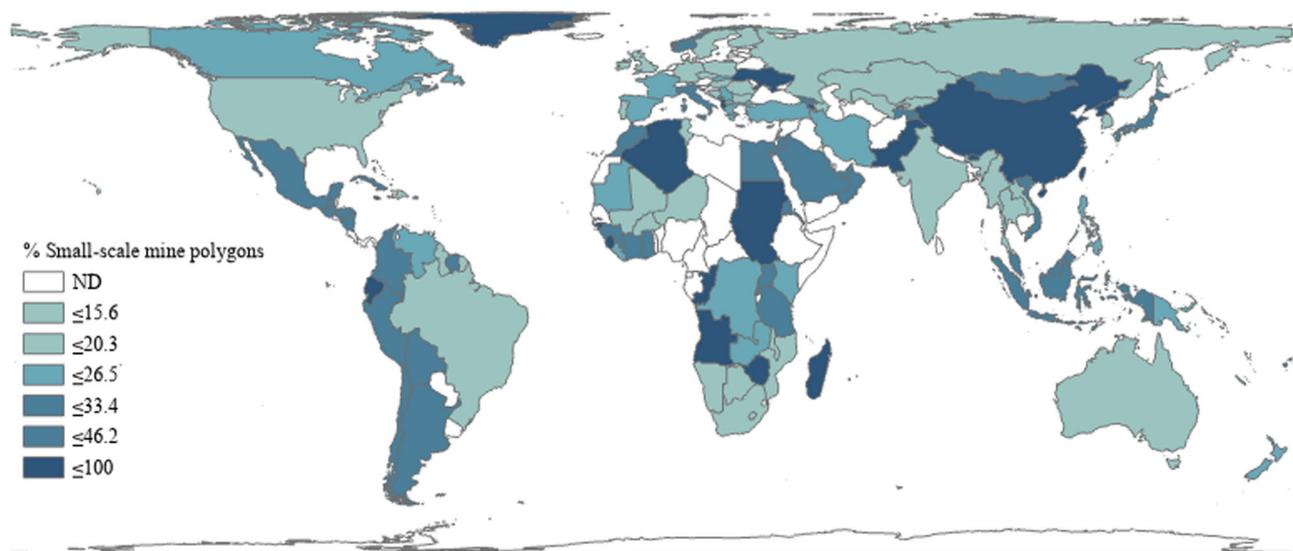
Fig. 4 Global distribution of small-scale mining polygons. Percentage of mine polygons <0.062 km^2 per country, signaling and validating an increased prevalence of ASM.

stages such that they appear as small-scale operations. Geographic restrictions that inhibit the expansion of mining, such as steep terrain and dense population[35], as well as minor ore bodies that limit larger-scale operations can also have an influence on the appearance of mine areas. Small coal-waste dumps in Ukraine are evidence of this[36]. Applying a marker of 0.062 km^2 per mine area (as the geometric mean of smaller scales), 27,410 polygons (36.8%) may be considered small scale (but not necessarily ASM), with the mean value of 0.024 km^2 accumulating only 665.3 km^2 in total (~1.0% of global mapped mining land use). Collectively, except for Guinea-Bissau with a limited mine sample size, North Korea exhibited the greatest proportion of small-scale mining in the world (74.4% of mine polygons). The majority of the smallest polygons are distributed in developing nations, including Sierra Leone, Albania, Algeria, Pakistan, and Angola. However, this is not a constant trait of all such countries. China hosts substantial small-scale mining, with ~16,676 small-scale mining polygons (53.5%) identified (Fig. 4).

Agricultural poverty, the potential to generate extensive distributional benefits, and customary land tenure practices may also be influential in encouraging informal mine operations[37,38]. Yet the average mine polygon size positively correlates with human development[8]. More developed countries with ample mineral resources exhibit lower percentages of small-scale mining, with an average percentage of 18.8% among countries like New Zealand, Canada, Australia, USA, and South Africa. This is likely attributable to planning and management practices that encourage larger scale operations, alongside access to technologies and equipment employed at larger scales[39]. The regulatory environment of developed countries can add to the cost of mining, creating conditions more favorable to larger scales[8]. In Russia, where only 13.4% of polygons may be considered small scale, larger reserves of mineral resources, or deposits otherwise classified as high grade are often prioritized for larger-scale developments (Fig. 4).

Comparisons, uncertainties and replicability. Comparing to previous studies mapping mine areas at national or global scales can help to identify what consistency or replicability has been achieved. A comparison of results from a sample of recent literature is presented in Table 3. Our current dataset represents 165% of the polygons of Maus et al.[18], while only indicating 65% of the total area. This is likely explained by Maus et al.[18] including spaces between adjacent mine features within an overall polygon shape, a difference

Table 3 Comparison of results with a sample of prior mine area studies.

Regions/scale	Mines/ Polygons	Occupied land (km²)	Average area[a] (km²)	Delineation for mine areas	Source
Global	62,381 (points with uniform buffers)	"Impacted land" 49.9 million	799	Impacted land is defined as extending up to 50 km from mine sites	6
Global	295 mines, with 3736 polygons	3633	12.3	Detailed manual delineation, classifying by mine feature type. Focuses explicitly on largest-scale operations.	3
Global	21,060 polygons	57,277	2.7	Manual delineation of mine areas utilizing a 10 km buffer from SNL coordinates, broadly encompassing mine areas, adjacent features	7
Global	24,605 polygons	31,396.3	1.3	Manual delineation. Draws tighter boundaries around mine features to explore variability in mine polygon shapes.	8
Global	44,929 polygons	101,583	1.8	Visual interpretation, per methods consistent with ref. 7	18
China	5189 polygons	1884.0	0.36	Manual delineation.	9
Brazilian Amazon	–	"Impacted land" 11,670	–	70 km beyond mining lease boundaries	5
Brazil	182 mines	2061	11.3	Data are presented in both raster format and as points with 5, 10, and 20 km buffers. Point data were used to	40
Brazil	–	101.7	–	New deforestation due to wildcat gold mining in 2020 only	27
Global	74,548 polygons	65,585.4	0.88 (0.123 geometric mean)	Visual interpretation, per methods consistent with ref. 8	Present study

[a]Arithmetic means of occupied mine land.

in methodology explored in Tang et al.[8]. Tang et al.[8] employ the same delineation methodology as this study, yet our study produces a 303% comparative polygon count for a 208% increase in total area. Our higher count of polygons per unit area may be explained by our increased coverage of small-scale mining (which often exhibit more numerous, smaller and dispersed features). ASM areas mapped in this study are subject to different land-use change dynamics, and can cumulatively represent a considerable land area, albeit representing a relatively smaller proportion of global mineral production. Within this subset, we also observe some differences to other studies. For example in Ghana, ~470 km² of vegetation has been reported as lost to mining, along with the expansion of artisanal mining[19]. In our study, we mapped 1003.8 km² of mine polygons in Ghana, supported by past studies identifying the location of 394 artisanal mining and 104 industrial mining sites for gold extraction in Ghana's southwestern forests[189].

Other studies also exhibit apparent dissimilarities to each other, albeit with different stated scopes. For example, Werner et al.[3], mapped 295 global metal mine sites (at ~28.2 km²/site), specifically focusing on delineating large-scale mines in a similar fashion to the present study. Sonter et al.[5] mapped 62,381 mine sites (as points) with 50 km buffers leading to 49.9 million km² of land potentially impacted (at ~799 km² per site). These comparisons show that variability in sampling and mapping methodology may lead to considerably different understandings of mine land use and impacts on landscapes. Each approach has benefits and drawbacks, e.g., it can be quite practical to use buffer tools to assign equal land area per site, as manual delineation efforts are considerably reduced[6,7]. However, this approach does not allow the complex boundaries of mines sites to be assessed.

The results of the MapBiomas initiative in Brazil[40] also highlight the effects of different mapping methodologies. Their inclusion of areas that might be termed mine "lands" (areas wherein mining activity is the primary land use) situated between and surrounding mine "features" (e.g., pits, waste rock disposal areas, tailings dams, etc) leads MapBiomas to report a total area of 2061 km² (lands) for Brazil (Table 3), versus 1395 km² (features) mapped in our study (Table 1). Additional visual comparisons between our data and that of MapBiomas are provided in supplementary Fig. S1, highlighting these differences.

Collectively, these comparisons highlight that definitions of mining as mine features, or as broader areas wherein mining activity takes place, or yet even broader areas of impact can lead to considerable differences in total calculated area. These comparisons also highlight that our capacity to evaluate the accuracy of mapped mine areas will vary between countries, depending on the local availability of corroborating sources.

A further source of uncertainty is that mine areas are highly dynamic. A mine lifecycle may involve periods of expansion followed by periods of reclamation or revegetation. Considering the many challenges faced in restoring ecological function at former mine sites[41–43], areas with vegetation cover may still be heavily impacted, raising questions as to whether such areas ought to still be classified as mining. Our visual inspection methods cannot detect such aspects. We are restricted to representing mine features to the extent that they are, or at least have recently been, visible in satellite imagery. Compounding these challenges, satellite imagery itself can have high temporal variability, such that the available imagery for a single mine can only be represented by a mosaic of multiple years. Depending on image availability at the time of analysis, this factor alone can lead to substantial differences between studies.

Under these caveats, our validation steps show that when a uniform mine area definition and delineation method are applied to the same image, 92% consistency in mapping of mine areas is achievable. This level of internal accuracy is consistent with past work[7,18].

Broader environmental impact potential. Examining the intersection of mines with protected areas, we identified 2558 boundary violations, totaling ~6232 km², or ~9.5% of all mine polygons. The potential impacts of these intersections is variable. For example, the largest intersection is a single 1355 km² area of the Atacama Desert designated as Ramsar wetland overlapping lithium brine operations. Such brine operations may encompass entire salt flats, but the direct influence of mining on wetlands can be unclear[44]. In other zones, such as in protected forests in Venezuela, visible traces of mine-associated deforestation indicate a much clearer attribution of impacts. Intersecting mine areas

spanned 147 different types of protected area categories, including state and national parks, Ramsar wetlands, and World Heritage areas. A global map of these intersections is shown in supplementary Fig. S2. These intersections raise concerns about the global environmental footprint of mining, yet they are compounded by the fact that mine areas can expand over time. Globally, about 58.1% of mine areas in our dataset are located in flat terrain areas[8].

Mines also exert influence well beyond the boundaries delineated in this study. This distinction between direct land use, and broader areas of induced impact (particularly environmental impact) is an important one[45,46]. It has been found, for instance, that in the open-cut pit Grasberg gold/copper mine in West New Guinea, forest losses can be >42 times larger than the mine itself[47]. Artisanal gold mining in the Peruvian Amazon was identified to cause nearly 1000 km^2 of deforestation[46]. A recent study on mining-induced deforestation in tropical regions also finds 3264 km^2 of directly induced forest loss[22].

To further illustrate the broader areas of impact arising from mining, we use the index R to express a ratio of an area of impact or influence to a mine area:

$$R = 100 \times \frac{Buffer\ zone}{Mine\ area} \qquad (1)$$

A *Buffer zone* refers to an extended region outside the mine area. By one measure, a 1 km buffer zone can broadly illustrate zones where the effects of a tailings pond collapse, the transportation of toxic elements, and/or immediate impacts on indigenous settlements, arable land, river quality, and transportation line are most notable[48,49]. Alternatively, a buffer zone of 50 km has also been argued as an appropriate measure of zones affected by mining activity[6,22]. These zones are by no means prescriptive, but can help to provide a sense of the scales of mine-associated impacts. To illustrate the effect of these assumptions in the context of our dataset, we adopted 1 and 50 km as the buffer distance to model the buffer zone variation from mine sites. The total (dissolved) buffer zone from 1 km is ~0.29 million km^2, and ~24.5 million km^2 from a 50 km buffer distance (see supplementary Fig. S3). The 50 km buffer area in our database is approximately half that of the 49.9 million km^2 footprint estimated in Sonter et al.[6]. This is likely because our study does not consider pre-operational deposits without current visible footprints, and does not approximate results to 1 km^2 grid cells. This comparison highlights the considerable potential for footprint estimates to increase as new deposits are developed, and as existing sites expand.

Meanwhile, the R collectively decreases with the extent of the mine area (decreasing ratio of land use to perimeter), revealing that small-scale mining causes a comparatively larger zone of influence per unit of mine area. It follows that large-scale mining may achieve economies of scale that result in reduced overall impacts on land. For ASM, a 1 km buffer distance yields $R = 7.80$/km^2 mine area (8352.3 km^2 buffer area, 1071.2 km^2 mine area, 4058 mine polygons). Large-scale mining yields $R = 1.09$/km^2 mine area (25,491.7 km^2 buffer area, 23,334.3 km^2 mine area, 761 mine polygons).

Contributions and further work. This study has sought to consolidate our understanding of the global extent of mining activity through extensive mapping and analysis of recent satellite imagery. By incorporating additional areas and types of mining activity, we have substantially updated previous global mine land-use datasets that focus on the specific contour of mine features. However, despite these efforts, it is evident that additional mining activity still remains to be assessed. This is likely because (1) production is ongoing at many of the sites mapped, leading to an

expected increase in the footprints of sites in our database, (2) exploration success will lead to the development of new sites, and (3) continued effort may yield further identification of unidentified sites. This is particularly so for mine areas operating under informal conditions, which we have primarily assessed on a case study basis, due to no complete global inventory of such sites available to guide our mapping. It was noted during validation that characteristically small aggregate quarry sites, particularly those operating in urban contexts, may also be underrepresented in our dataset. Given these challenges, a necessary future advancement will be to automate mapping processes through the development of advanced machine learning technology that can recognize mine features and appropriately classify them in satellite imagery, despite their visual and spectral heterogeneity. The database provided here may be an invaluable training dataset toward such an endeavor.

Materials and methods
This study demonstrates a replication of previously established methods for identifying and delineating mine areas in satellite imagery. These methods are described at length in refs. [3,7,8], but are also expanded upon here.

Identification of mine sites. To identify the location of mine sites, we conducted an online literature review comprising published literature, government and industry publications, and corporate and national mining databases. In cases where coordinates of a mine or minefield were not provided (e.g., from sources such as mindat.org, or the SNL database), but qualitative descriptors were available (e.g., proximity to known landmarks), then visual inspection of satellite imagery was used to support site identification. As this study expands upon previous global mine area research, we also re-examined previously mapped mining regions to determine if global coverage could be improved or updated. Specifically, we identified additional sites by (1) using navigation tools in Google Earth Pro to scan imagery of likely locations adjacent to existing known features, and (2) expanding the analysis of countries previously underrepresented in past studies. This process was further aided by considering factors like potential adjacent coal mines for coke supply of iron smelters, or areas within surrounding zones of mineralization, such as faults (e.g., quartz-vein-type gold ore), orogenic belts (e.g., porphyry copper deposit), and sedimentary basins (e.g., coal mines), including a small proportion of unidentified waste disposal and dumping sites, deposits of surficial mines, cessation tailings ponds, and affiliated mineral processing facilities (see supplementary Fig. S4 for examples).

Prior studies have been limited in their spatial coverage by focusing primarily on regulated/formal mining activity, yet ~40–100 million people are estimated to depend on small-scale mining for their livelihoods[28,29], indicating a potential for cumulatively large mine areas that require mapping. The recent update from Maus et al.[18] has also sought to address this. More ASM sites were identified in this study using high-resolution remote sensing images visible in Google Earth Pro and Sentinel II, particularly in Africa and Latin America (see ref. [50]). A challenge of including such areas is that formal documentation of these sites is seldom available, adding uncertainty to the identification of such mine sites and limiting opportunities for verification/validation. We nonetheless identified sites where ASM features were highly recognizable, considering aspects like the structure, location, color, texture, composition, topography, mine type, local industry type, and evidence of pollutants. For example, for placer gold mining in Ofin River, Ghana, the turbid river water and the highly reflective areas along the river render mining activity in this region quite distinctive (see Fig. 1).

Delineation of mine feature polygons. Once mine site locations were known, polygons outlining mine features were drawn where recent and adequately well-defined Google Earth imagery was available, such that mine areas were possible to distinguish from their surrounds.

To delineate mine areas, the authors drew upon extensive experience in recognizing mine features in satellite imagery[3,4,8,9]. Although it is noted that a mine site can be composed of a diverse range of features, we focused primarily on delineating features that relate primarily to the core functioning of the sites, such as open cut pits, tunnel entrances, ore stockpiles, heap leach pads, waste rock disposal areas, infrastructure areas, tailings storage facilities and water ponds. This excludes downstream processing facilities such as smelters, refineries, unless they were also co-located with on-site milling/beneficiation infrastructure. We did not seek to delineate areas of impact arising from such features, for example gaseous of liquid wastes arising from such features, or secondary/tertiary land use changes emerging from the presence of a mine. Revegetated areas, backfilled pits, or pits subsequently employed for water storage were identified using historical imagery as well as public reports, such as news articles or company publications. We only delineated infrastructure areas that were clearly related to mineral production, therefore generally excluding features like roads and railways. In cases where mines operated
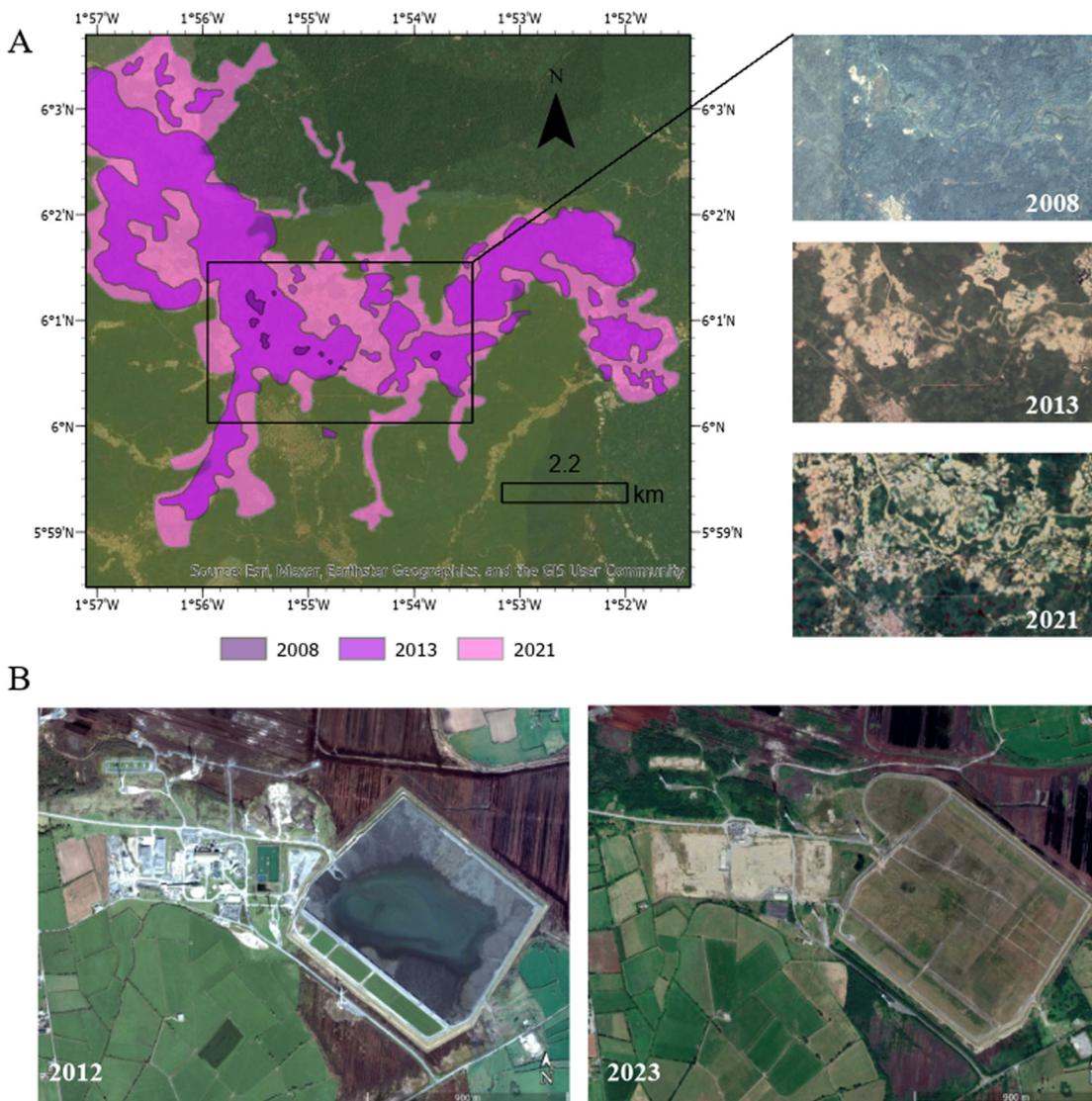
Fig. 5 The changing spatiotemporal characteristics of mine areas. A Spatiotemporal variation of ASM areas (placer gold mining, Ofin River, Ghana 6°1′00″ N, 1°52′27″ W). Image © 2023 CNES/Airbus and Maxar Technologies, visualized in Google Earth Pro. **B** Cessation mine tailings in the Lisheen Mine, Ireland. This mine was operational in 2012 and increasing vegetation cover is evident in 2023 (lead-zinc-silver mine; 52°45′01″ N, 7°40′35″ W). Images © 2023 CNES/Airbus, visualized in Google Earth Pro.

close to built-up areas, this process entailed distinguishing milling infrastructure from surrounding buildings. Areas were delineated manually using polygon tools and publicly available imagery in Google Earth Pro. Depending on the location, this imagery varied in resolution. For example, some rural areas only receive coverage from SPOT satellites where resolution from 1.5 to 10 m is achieved. Ikonos imagery may cover other zones at 1 m resolution. Other services, including WorldView-1 to 3 and GeoEye-1 achieve a resolution of 0.5 m, and in some parts of Japan, North America and Europe, imagery is available from localized sources (e.g., aerial imagery) that achieve 0.15 m resolution. Assessing these images, we considered aspects like texture, color (e.g., reflectance of exposed rock versus surrounding vegetation), composition (positioning within the landscape), topography (determining whether the presence of such a feature makes sense given the surrounding terrain), light (e.g., identifying shadows cast from pits of rack of dumps) and overall form (recognizing familiar features as a whole) to manually draw boundaries. We aimed to maintain polygon boundaries that closely contoured the form of specific mine features, as seen in Fig. 1A. The location and global coverage of sites mapped in this study are shown in Fig. 1. It includes both currently active mines and abandoned and historic mine sites[35].

Historical satellite imagery available in Google Earth Pro was also assessed to cross-check areas, particularly if newer imagery was obscured by low resolution or cloud cover. This also enabled the identification and verification of some closed mine sites and closed tailings ponds in Japan, the United States, and Europe, where substantial mining activity is known to have taken place in the early- and mid-20th century. Many of these areas, notably some coal extraction areas in Germany, Poland, Belgium, and lead-zinc areas in Ireland, exhibited characteristics of

processes of ecological restoration (Fig. 1, supplementary Fig. S4). Some coal disposal areas in China are notable for their transition to agricultural land uses, presenting an increased risk of classification uncertainty (see ref. [3]).

Where available, additional literature or imagery (e.g., company websites, aerial photographs, technical reports, or Landsat imagery) were examined to verify features that remained unclear to authors after initial cross-checking. Notwithstanding these efforts, the process of delineating mine areas is subject to inherent uncertainties such as incorrect interpretation/classification, temporal variation in the landscapes mapped, and precision of the satellite images (see ref. [3]). The imagery assessed via Google Earth has an overall positional root mean squared error (RMSE) of 39.7 m related to the reality on the ground[51,52], which has been considered for past global scale mine area analyses[8]. All polygons were converted to a projected coordinate system (WGS 1984 EASE Grid Global). Post-processing checks were conducted to identify invalid polygons (e.g., empty mine areas or distorted boundaries) and repair geometry to ensure polygons are accurate.

Additional data validation. To verify that mine areas were correctly delineated, we used ground photography and GPS coordinates obtained from recent and past field excursions in China (Panzhihua, and Ordos), Germany (Harz Mountain), and Australia (North-west Tasmania), and utilized an external reviewer to replicate and compare output maps.

The most recent available remote sensing imagery for mapping was used as a first preference, recognizing the potential for sites to grow over time (Fig. 5A). The effects of a dynamically changing landscape, and hence issues of changing

Table 4 Distribution of validation polygons.

	200 validation polygons	348.2 km^2
	The present study	322.2 km^2
Countries	Ukraine (51), Democratic Republic of Congo (43), Suriname (23), China (12), Zambia (12), Finland (10), Sweden (7), Germany (6), French Guiana (6), Brazil (5), Estonia (5), Mozambique (5), Czech (3), Guinea (3), Poland (3), The former Yugoslav Republic of Macedonia (2), Russia (2), France (1) and Mauritania (1).	
Climate	Tropical (39), Dry (4), Temperate (70), Cold (87) and Polar (0).	Climate classification based on[59]
Topography	Mountains (41) and Plains (159).	Terrain classification based on[60]

vegetation cover (either naturally or as part of concerted restoration efforts) obscuring operational boundaries are shown in (Fig. 5B).

We validated and updated mine area datasets of 24,605 polygons (33%) from Tang et al.[8] to match more recent imagery where available, and newly delineated 49,943 additional mine area polygons (66%) for the present study. The independent delineation of mine areas from an volunteer reviewer sought to represent different countries, climate divisions, and topography. The reviewer, Dr. Yang Jingsong, is familiar with the application of mine delineation methods as described here, and as used in the previous iteration of our database[8]. Their outputs are summarized in Table 4 and a visualization of their polygons in provided in supplementary Fig. S5. We found that there was ~92% agreement between mapped areas, suggesting that our global estimates could vary in the order of ±8% through the propagation of human error. This also highlights that even the application of consistent delineation criteria cannot guarantee full replicability in total areas, however the overall location and magnitude of impacted areas remains broadly consistent.

Spatial analysis. Following delineation, ArcGIS 10.8 and ArcGIS Pro 2.4.0 programs were used to assess spatial attributes of the mine areas dataset and the concurrence of human and environmental overlays. Using the SNL database, we applied 10 km buffers (consistent with Maus et al.[7,18]) to point locations of mine operations. We then performed a spatial overlay (intersection) analysis to identify the area of polygons that sit within these buffers, and hence determine the number and type of mine operations potentially represented by our dataset. The World Database on Protected Areas[53,54] was also downloaded to ArcGIS Pro 2.4.0, and a spatial overlay analysis was performed using a the spatial join and intersect tools to identify the extent of overlap between protected areas and mine polygons. This allowed us to determine the extent that mining may induce impacts on environmentally sensitive regions.

The Global and Local Moran's I indices were employed to examine the spatial distribution characteristics of the mine areas. The Anselin Moran's I is a commonly used indicator of spatial autocorrelation (clustering behavior) based on the Pearson correlation coefficient. The Global Moran's I index is used to study the degree of autocorrelation for the dataset as a whole, while the local indicators of the spatial association are applied to identify specific locations that exhibit different clustering behaviors[55]. Such areas may then be visualized via GIS[56]. The test employed 9999 permutations in this study, with $p < 0.05$. A strong positive Local Moran's I value indicates that the location under study has similarly high or low values to its neighbors. Conversely, a strong negative Local Moran's I value implies that the sites under investigation are significantly different from the values of their surrounding locations, indicating areas of unusually high or low clustering of mine areas relative to their surrounds. The global spread of mining activity can be distinguished according to statistically significant clusters of: high density (HH), low density (LL), outliers of high density surrounded by low density (HL), and outliers of low density surrounded by high density (LH). Further explanations of these categories are provided by[55] and[57]. A 'Not Significant' (NS) classification represents highly isolated or completely absent mining, and is evident across many high altitude, alpine, and arid regions (e.g., Central Asian Orogenic Belt, Andes Belt, Northern Europe). LL regions are often associated with higher population density, hence minimizing land available for extraction. Agricultural land, transportation lines, and topographical restrictions may also artificially subdivide a minefield into multiple, lower-density mine sections. Such regions include parts of Eastern China (e.g., polymetallic metal mining), Western USA (e.g., with some coal mining in the Appalachian Mountains), India (e.g., iron ore mining), and the east coast of Brazil (e.g., iron ore mining). HL zones are situated within the LL pattern boundaries or NS areas. They represent high density mining activity with statistically low-density surrounds. Zones of significant mine area density, surrounded by yet more significant mining activity constitute a HH cluster. These regions were characteristically lower population density. Examples of such areas included Western Australia (e.g., Tropicana gold mine), Queensland, Australia (e.g., Mount Isa copper, lead, zinc, and silver mine), Magadanskaya Oblast, Russia (gold), Chukotskiy Avtonomnyy Okrug, Russia (gold, diamond) and Bolivia (San

Cristóbal silver, lead and zinc mine). Within HH areas, we may identify some LH regions of notably low mine site density. Such areas may feature within highly mineralized belts, such as the Andes, where mine areas appear in relative abundance, yet geographical factors like steep mountain ridges prevent parts of these belts from being developed.

Data availability
The spatial data that support the findings of this study are available from https://doi.org/10.5281/zenodo.6806817.

References
1. Bebbington, A., Hinojosa, L., Bebbington, D. H., Burneo, M. L. & Warnaars, X. Contention and ambiguity: Mining and the possibilities of development. *Dev. Change* **39**, 887–914 (2008).
2. Mudd G. M., et al. Critical Minerals in Australia: A Review of Opportunities and Research Needs. (Geoscience Australia, Canberra, 2019). https://doi.org/10.11636/Record.2018.051.
3. Werner, T. T., Mudd, G. M., Schipper, A. M., Huijbregts, M. & Northey, S. A. Global-scale remote sensing of mine areas and analysis of factors explaining their extent. *Global Environ. Change* **60** https://doi.org/10.1016/j.gloenvcha.2019.102007 (2020).
4. Werner, T. T. A Geospatial Database for Effective Mine Rehabilitation in Australia. *Minerals* **10**, 745 (2020).
5. Sonter, L. J. et al. Mining drives extensive deforestation in the Brazilian Amazon. *Nat. Commun.* **8**, 1–7 (2017).
6. Sonter, L. J., Dade, M. C., Watson, J. E. M. & Valenta, R. K. Renewable energy production will exacerbate mining threats to biodiversity. *Nat. Commun.* **11**, 4174 (2020).
7. Maus, V. & Giljum, S. a global-scale data set of mining areas. *Sci. Data* https://doi.org/10.1038/s41597-020-00624-w (2020).
8. Tang, L., Tim, T. W., Xie, H., Yang, J. & Shi, Z. A global-scale spatial assessment and geodatabase of mine areas. *Global Planetary Change* **204**, 103578 (2021).
9. Tang, L., Liu, X., Wang, X., Liu, S. & Deng, H. Statistical analysis of tailings ponds in China. *J. Geochem. Explor.* **216**, 106579 (2020).
10. Asner, G. P., Llactayo, W., Tupayachi, R. & Luna, E. R. Elevated rates of gold mining in the Amazon revealed through high-resolution monitoring. *Proc. Natl Acad. Sci. USA* **110**, 18454–18459 (2013).
11. Northey, S. A. et al. The exposure of global base metal resources to water criticality, scarcity and climate change. *Global Environ. Change* **44**, 109–124 (2017).
12. Sonter, L. J., Ali, S. H. & Watson, J. E. M. Mining and biodiversity: key issues and research needs in conservation science. *Proc. Biol. Sci.* **285**, 20181926 (2018).
13. S&P Global Market Intelligence. SNL Metals and Mining Database. https://www.spglobal.com/marketintelligence/en/campaigns/metals-mining. (2018).
14. Mudd, G. M. Assessing the Availability of Global Metals and Minerals for the Sustainable Century: From Aluminium to Zirconium. *Sustainability* **13**, 10855 (2021).
15. Mudd, G. M. & Jowitt, S. M. Growing Global Copper Resources, Reserves and Production: Discovery Is Not the Only Control on Supply. *Econ. Geol.* **113**, 1235–1267 (2018).

16. Yang, Y. et al. Detecting the dynamics of vegetation disturbance and recovery in surface mining area via Landsat imagery and LandTrendr algorithm. *J. Cleaner Product.* **178**, 353–362 (2018).

17. Yu, X., Zhang, K. & Zhang, Y. Land use classification of open-pit mine based on multi-scale segmentation and random forest model. *PLOS ONE* **17**, e0263870 (2022).

18. Maus, V. et al. An update on global mining land use. *Sci. Data* **9**, 433 (2022).

19. Barenblitt, A. et al. The large footprint of small-scale artisanal gold mining in Ghana. *Sci. Total Environ.* **781**, 146644 (2021).

20. ESRI. *Create Fishnet (Data Management)*, https://pro.arcgis.com/en/pro-app/latest/tool-reference/data-management/create-fishnet.htm (2022).

21. Butt, N. et al. Conservation. Biodiversity risks from fossil fuel extraction. *Science* **25**, 425–426 (2013).

22. Giljum, S. et al. A pantropical assessment of deforestation caused by industrial mining. *Proc. Natl Acad. Sci.* **119**, e2118273119 (2022).

23. Walsh, S. D., Northey, S. A., Huston, D., Yellishetty, M. & Czarnota, K. Bluecap: A geospatial model to assess regional economic-viability for mineral resource development. *Resourc. Policy* **66**, 101598 (2020).

24. Huo, X.-N. et al. Combining Geostatistics with Moran's I Analysis for Mapping Soil Heavy Metals in Beijing, China. *Int. J. Environ. Res. Public Health* **9** https://doi.org/10.3390/ijerph9030995 (2012).

25. Wu, Y., Chen, J., Zheng, C., Wei, F. & Adriano, D. C. Background concentrations of elements in soils of China. *Water Air Soil Pollut.* **57-58**, 699–712 (1991).

26. Hentschel, T., Hruschka, F. & Priester, M. 2002. Global report on artisanal and small-scale mining. Report commissioned by the Mining, Minerals and Sustainable Development of the International Institute for Environment and Development. http://www.iied.org/mmsd/mmsd_pdfs/asm_global_report_draft_jan02.pdf, 20 (08), 2008.

27. Siqueira-Gay, J. & Sánchez, L. E. The outbreak of illegal gold mining in the Brazilian Amazon boosts deforestation. *Region. Environ. Change* **21**, 28 (2021).

28. Lottermoser, B. G. Mine Wastes. *Characterization, Treatment and Environmental Impacts* https://doi.org/10.1007/978-3-642-12419-8 (2010).

29. Kossoff, D. et al. Mine tailings dams: Characteristics, failure, environmental impacts, and remediation. *Appl. Geochem.* **51**, 229–245 (2014).

30. Kaninga, B. K. et al. Review: mine tailings in an African tropical environment—mechanisms for the bioavailability of heavy metals in soils. *Environ. Geochem. Health* **42**, 1069–1094 (2020).

31. Shandro, J. A., Veiga, M. M. & Chouinard, R. Reducing mercury pollution from artisanal gold mining in Munhena, Mozambique. *J. Cleaner Product.* **17**, 525–532 (2009).

32. Hilson, G. Abatement of mercury pollution in the small-scale gold mining industry: Restructuring the policy and research agendas. *Sci. Total Environ.* **362**, 1–14 (2006).

33. Drace, K. et al. Mercury-free, small-scale artisanal gold mining in Mozambique: utilization of magnets to isolate gold at clean tech mine. *J. Cleaner Product.* **32**, 88–95 (2012).

34. Malpeli, K. C. & Chirico, P. G. The influence of geomorphology on the role of women at artisanal and small-scale mine sites. *Nat. Resourc. Forum* **37**, 43–54 (2013).

35. Li, X., Yang, F., Peng, X., Li, H. & Tang, L. Risk assessment of small scale mining waste dump: a case study of Jialing River Basin (In Chinese). *Resourc. Environ. Yangtze Basin* **30**, 2755–2762 (2021).

36. Nádudvari, Á. et al. Self-Heating Coal Waste Fire Monitoring and Related Environmental Problems: Case Studies from Poland and Ukraine. *J. Environ. Geogr.* **14**, 26–38 (2021).

37. Ofosu, G., Dittmann, A., Sarpong, D. & Botchie, D. Socio-economic and environmental implications of Artisanal and Small-scale Mining (ASM) on agriculture and livelihoods. *Environ. Sci. Policy* **106**, 210–220 (2020).

38. Banchirigah, S. M. Challenges with eradicating illegal mining in Ghana: A perspective from the grassroots. *Resourc. Policy* **33**, 29–38 (2008).

39. Iwatsuki, Y., Nakajima, K., Yamano, H., Otsuki, A. & Murakami, S. Variation and changes in land-use intensities behind nickel mining: Coupling operational and satellite data. *Resourc. Conser. Recycling* **134**, 361–366 (2018).

40. Azevedo Sr, T., Souza Jr, C., Shimbo, J. & Alencar, A. MapBiomas initiative: Mapping annual land cover and land use changes in Brazil from 1985 to 2017. American Geophysical Union, Fall Meeting 2018, Washington D.C., USA, Dec 10-14, 2018. Abstract #B22A-04 *AGU Fall Meeting Abstracts*.

41. Rosa, J. C., Morrison-Saunders, A., Hughes, M. & Sánchez, L. E. Planning mine restoration through ecosystem services to enhance community engagement and deliver social benefits. *Restor. Ecol.* **28**, 937–946 (2020).

42. Li, M. Ecological restoration of mineland with particular reference to the metalliferous mine wasteland in China: a review of research and practice. *Sci. Total Environ.* **357**, 38–53 (2006).

43. Chen, Z. et al. Ecological restoration in mining areas in the context of the Belt and Road initiative: Capability and challenges. *Environ. Impact Assess. Rev.* **95**, 106767 (2022).

44. Moran, B. J. et al. Relic groundwater and prolonged drought confound interpretations of water sustainability and lithium extraction in arid lands. *Earth's Future* **10**, e2021EF002555 (2022).

45. Asner, G. P. & Tupayachi, R. Accelerated losses of protected forests from gold mining in the Peruvian Amazon. *Environ. Res. Lett.* **12**, 094004 (2017).

46. Caballero Espejo, J. et al. Deforestation and Forest Degradation Due to Gold Mining in the Peruvian Amazon: A 34-Year Perspective. *Remote Sensing* **10**, 1903 (2018).

47. Alonzo, M., Van Den Hoek, J. & Ahmed, N. Capturing coupled riparian and coastal disturbance from industrial mining using cloud-resilient satellite time series analysis. *Sci. Rep.* **6**, 35129 (2016).

48. Wang, K. et al. Integration of DSM and SPH to Model Tailings Dam Failure Run-Out Slurry Routing Across 3D Real Terrain. *Water* **10** https://doi.org/10.3390/w10081087 (2018).

49. Kun, W., Peng, Y., Hudson-Edwards, K., Wen-sheng, L. & Lei, B. Status and development for the prevention and management of tailings dam failure accidents. *Chinese J. Eng.* **40**, 526–539 (2018).

50. Djibril, K. N. G. et al. Artisanal gold mining in Batouri area, East Cameroon: Impacts on the mining population and their environment. *J. Geol. Mining Res.* **9**, 1–8 (2017).

51. Potere, D. Horizontal Positional Accuracy of Google Earth's High-Resolution Imagery Archive. *Sensors* **8**, 7973–7981 (2008).

52. Olofsson, P. et al. Good practices for estimating area and assessing accuracy of land change. *Remote Sensing Environ.* **148**, 42–57 (2014).

53. Hanson, J. O. wdpar: Interface to the World Database on Protected Areas. *J. Open Source Softw.* **7**, 4594 (2022).

54. Bingham, H. C. et al. Sixty years of tracking conservation progress using the World Database on Protected Areas. *Nat. Ecol. Evol.* **3**, 737–743 (2019).

55. Anselin, L. Local Indicators of Spatial Association-LISA. *Geogr. Analys.* **27**, 93–115 (1995).

56. Harries, K. Extreme spatial variations in crime density in Baltimore County, MD. *Geoforum* **37**, 404–416 (2006).

57. Mitchel, A. The ESRI Guide to GIS analysis, Volume 2: Spartial measurements and statistics. *ESRI Guide to GIS analysis* (2005). ISBN:9781589486089, 1589486080

58. Li, X.-y., Yang, F., Xiu-hong, P., Li, H.-l. & Tang, L. Security Assessment of Mining Wastes in Jialing River Basin-Indicative Significance for Small-scale Storage Yards (in Chinese). *Resour. Environ. Yangtze Basin* **30**, 2755–2762 (2021).

59. Peel, M. C., Finlayson, B. L. & McMahon, T. A. Updated world map of the Köppen-Geiger climate classification. *Hydrol. Earth Syst. Sci.* **11**, 1633–1644 (2007).

60. Sayre, R. et al. A New High-Resolution Map of World Mountains and an Online Tool for Visualizing and Comparing Characterizations of Global Mountain Distributions. *Mountain Res. Dev.* **38**, 240–249 (2018).

Acknowledgements

Author contributions

L.T.: Conceptualization, Methodology, Investigation, Visualization, Writing—original draft. T.W.: Methodology, Investigation, Visualization, Supervision, Writing—original draft, Writing—review & editing.

Competing interests

The authors declare no competing interests.

Additional information

Supplementary information The online version contains supplementary material available at https://doi.org/10.1038/s43247-023-00805-6.

Correspondence and requests for materials should be addressed to Tim T. Werner.

Peer review information *Communications Earth & Environment* thanks Luis Enrique Sanchez, Susmita Sharma and the other, anonymous, reviewer(s) for their contribution to the peer review of this work. Primary Handling Editors: Sadia Ilyas and Joe Aslin.

Reprints and permission information is available at http://www.nature.com/reprints

Publisher's note Springer Nature remains neutral with regard to jurisdictional claims in published maps and institutional affiliations.

Terms and Conditions